AIP | The Journal of Chemical Physics

A highly accurate and efficient algorithm for electrostatic interactions of charged particles confined by parallel metallic plates

Samare Rostami, S. Alireza Ghasemi, and Ehsan Nedaaee Oskoee

Citation: The Journal of Chemical Physics **145**, 124118 (2016); doi: 10.1063/1.4963667
View online: http://dx.doi.org/10.1063/1.4963667
View Table of Contents: http://scitation.aip.org/content/aip/journal/jcp/145/12?ver=pdfcov
Published by the AIP Publishing

A highly accurate and efficient algorithm for electrostatic interactions of charged particles confined by parallel metallic plates

Samare Rostami, S. Alireza Ghasemi,[a] and Ehsan Nedaaee Oskoee
Institute for Advanced Studies in Basic Sciences, P.O. Box 45195-1159, Zanjan, Iran

(Received 21 June 2016; accepted 13 September 2016; published online 30 September 2016)

We present an accurate and efficient algorithm to calculate the electrostatic interaction of charged point particles with partially periodic boundary conditions that are confined along the non-periodic direction by two parallel metallic plates. The method preserves the original boundary conditions, leading to an exact solution of the problem. In addition, the scaling complexity is quasilinear $O(N\ln(N))$, where N is the number of particles in the simulation box. Based on the superposition principle in electrostatics, the problem is split into two electrostatic problems where each can be calculated by the appropriate Poisson solver. The method is applied to NaCl ultra-thin films where its dielectric response with respect to an external bias voltage is investigated. Furthermore, the total charge induced on the metallic boundaries can be calculated to an arbitrary precision. *Published by AIP Publishing.* [http://dx.doi.org/10.1063/1.4963667]

I. INTRODUCTION

A recurring problem in physics and chemistry experiments is the study of an ionic material with slab like geometry, sandwiched between two parallel metallic plates at two different electric potentials.[1] Commonly, such a configuration is encountered in solid oxide fuel cells and batteries where an electrolyte is used between two electrodes as well as in capacitors with a dielectric. Atomistic simulations are of great importance to gain a better understanding of the microscopic mechanisms and processes involved in such systems. The electrostatic interaction in ionic materials dominates the interatomic forces and its proper calculation is therefore essential when simulating electrolytes and dielectrics. Electrostatic terms play a significant role in many advanced atomistic potentials[2] such as ReaxFF reactive force field which can be used in atomistic simulation of membranes.

Commonly, the effect of the two electrodes in atomistic simulation of electrolytes is modeled by an external uniform electric field perpendicular to the surface. Such an approximation does not provide information on various physical properties such as the charge density induced at the electrodes and the microscopic response of particles in the vicinity of the interface between the electrolyte and the electrodes. In addition, the effect of an external uniform electric field may be different from the electrostatic interaction in the electrolyte with the presence of the two electrodes, in particular when the electrolyte is ultrathin. Furthermore, possible nonlinear effects cannot be captured at all when using a uniform electric field.

The efficient calculation of the electrostatic interactions of point particles is not a trivial task. For free boundary conditions, the direct summation of the particle interaction scales as $O(N^2)$ due to the long ranged nature of the Coulomb potential, where N is the number of particles in the simulation cell. Several methods[3,4] have been developed for the calculation of the Coulomb interaction with free boundary conditions that have a complexity of $O(N\ln(N))$ while preserving the original boundary conditions without introducing any gap in the non-periodic direction. On the other hand, for fully periodic boundary conditions, all periodic images of the particles in the simulation cell must be considered alongside the original particles. The Ewald method,[5] which is commonly used for such systems, has the scaling complexity of $O(N^2)$, which can be improved to $O(N^{\frac{3}{2}})$ by choosing optimal parameters. The scaling can be even further enhanced to $O(N\ln(N))$ if fast Fourier transformation (FFT) is employed.

For a proper investigation of materials with slab like geometries, the lateral directions must be treated with periodic boundary conditions and free boundary condition needs to be used for the perpendicular, non-periodic direction. This type of boundary condition is typically also referred to as surface, slab, or 2D+h boundary condition. Several approaches have been followed to treat Coulombic interaction with such surface boundary conditions. Some are based on the MMM method,[6] and its adaption for slab boundary conditions is called MMM2D.[7] Although it can treat the slab boundary condition exactly, the scaling complexity is inefficient and behaves like $O(N^{\frac{5}{3}})$. Other more popular methods are in the spirit of the Ewald method,[8–16] and the standard implementation based on FFT has been widely used in atomistic simulations. The major problem of the standard Ewald approach arises from the assumption that the boundary conditions in all three dimensions are periodic. Therefore, the non-periodic direction must be treated by including a vacuum space to decouple the interaction between the particles in the simulation cell and their periodic images. This approach not only makes the method inefficient but the interaction between periodic images does not decay fast enough with the size of the vacuum layer if the system has a non-vanishing dipole moment. Recently,

[a]aghasemi@iasbs.ac.ir

methods such as particle particle particle mesh with layer correction[9,10] (P3MLC) have been proposed to correct for the dipole-dipole interaction between periodic images. Ghasemi *et al.* introduced a method called particle particle particle density (P^3D) method,[8] which employs plane waves for the periodic directions and finite element for the non-periodic direction to expand the potential function and the charge density. The P^3D method is the only method to date which not only preserves the original slab boundary condition but also has a desirable scaling of $O(N \ln(N))$.

None of the aforementioned methods in their original form can be directly employed for the electrostatic calculation of charged particles confined by metallic boundaries. In recent years, some methods were developed by Holm *et al.*[17–19] to compute electrostatic interactions of charged particles confined between two dielectric materials. Although these methods have been originally developed for the electrostatic interaction of charged particles in media with a finite dielectric contrast, they can be used also in metallic boundaries by considering large permittivity for the surrounding dielectric. The induced charge MMM2D (ICMMM2D) method[17] is an extension of MMM2D and can treat planar dielectric interfaces by using image charge particles (ICP). In ICMMM2D, the number of ICPs strongly depends on the difference between dielectric constant of the electrolyte and of the surrounding materials. The computational cost of including ICPs scales linearly with the number of particles in the simulation box. However, for large number of particles in the cell, the original scaling of MMM2D is preserved. Based on the induced charge computation[20] (ICC) method, Tyagi *et al.*[18] introduced a generic method that can be used for dielectric interfaces of arbitrary shapes. The method requires a Poisson solver suitable for the same geometry in the absence of the dielectric interface. The method is called ICC*, in which the star denotes a place holder for any Poisson solver. The ICC* algorithm scales basically like the Poisson solver employed in the method. In 1989, Hautman[21] introduced a method for the electrostatic interaction of charged and polar particles between metallic plates. The method is an extension of the Ewald method which accounts for the effect of image particles.[21–23]

In this paper, we present a method based on the superposition principle in electrostatics to calculate electrostatic interactions of charged point particles between two parallel metallic plates. In fact, similar approaches can be applied to electrostatic interactions of charged point particles or continuous charge densities trapped by metallic boundaries of arbitrary shapes. However, here we focus on systems with slab geometry and show the particular advantage of the method for this type of geometry. The method scales basically like the Poisson solver of the problem in the absence of the metallic plates (exactly like ICC*). Here we employ the P^3D method;[8] thus, the algorithm scales like $O(N \ln(N))$. Furthermore, the proposed method offers improved accuracy and the electrostatic energy, forces, and other physical quantities of interest such as the total induced charge on the electrodes can be computed to an arbitrary precision.

II. METHOD

A. Splitting the electrostatic problem based on the superposition principle

Consider a system of N charged particles in a rectangular simulation box of dimensions L_x, L_y, and L_z with periodic boundary conditions in x and y directions. In order to model the electrodes, boundary conditions at $z = 0$ and $z = L_z$ are at constant voltages of V_{lp} and V_{up}, respectively. In fact, $\Delta V = V_{up} - V_{lp}$ indicates the potential difference between the two electrodes. The electrostatic interaction of charged particles with such boundary conditions is not Coulombic since the $\frac{1}{r}$-function does not satisfy the boundary conditions at $z = 0$ and $z = L_z$. The electric potential must fulfill the Poisson equation,

$$\nabla^2 V(\mathbf{r}) = -4\pi\rho(\mathbf{r}), \tag{1}$$

where $\rho(\mathbf{r})$ is the charge density of the point particles. The Green's function of the Poisson equation for a slab geometry with metallic boundary conditions is complicated and no compact functional form is known.

We propose a method based on the superposition principle in electrostatics that can be used for calculating the electrostatic interaction of charged particles or continuous charge densities surrounded with a metallic environment. Since the Poisson equation is a linear differential equation, the superposition principle applies in electrostatics and allows us to split the problem into two (see Fig. 1). The corresponding electric potentials of the two problems, which we call $V_1(\mathbf{r})$ and $V_2(\mathbf{r})$, fulfill the Poisson equation with two different charge densities, $\rho_1(\mathbf{r})$ and $\rho_2(\mathbf{r})$, respectively. The boundary conditions of the two problems also differ. Both the new

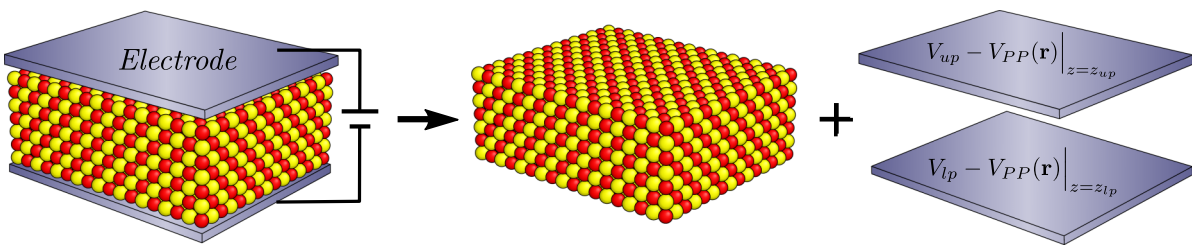

FIG. 1. Schematic illustration of the method where the electrostatic interaction of charged point particles confined by parallel metallic plates (left) is split into two parts; a system of charged point particles with free boundary condition in the z direction and periodic in x and y directions, (middle) and two parallel metallic plates with boundary conditions given in Eq. (2) (right).

charge densities and boundary conditions are arbitrary and can be anything, provided that $\rho(\mathbf{r}) = \rho_1(\mathbf{r}) + \rho_2(\mathbf{r})$ and the two boundary conditions sum up to the original boundary condition. Although this approach can be applied to any systems with metallic boundary conditions of arbitrary shape, we focus on systems with slab like geometries here. Charge densities $\rho_1(\mathbf{r})$ and $\rho_2(\mathbf{r})$ must be chosen such that the corresponding Poisson equations can be solved with available methods. Here we choose $\rho_1(\mathbf{r}) = \rho(\mathbf{r})$ and $\rho_2(\mathbf{r}) = 0$, while for the first problem the boundary conditions are taken to be free in z direction and periodic in x and y directions. In order to determine the boundary condition of the second problem, one needs to first solve the first problem. In this way, any Poisson solver can be employed that can treat slab like geometries, some of which are discussed in Sec. I. The Poisson solver of the first problem must provide potential values at the boundaries. From here on, $V_1(\mathbf{r})$ and $V_2(\mathbf{r})$ are replaced by $V_{pp}(\mathbf{r})$ and $V_s(\mathbf{r})$, respectively, to emphasize that the first problem is the electric potential due to charged point particles and the second problem is a smooth potential which does not diverge at any point within the simulation cell. Once $V_{pp}(\mathbf{r})$ is calculated, the Laplace equation of the second problem can be solved with the following boundary conditions:

$$V_s(\mathbf{r})\Big|_{\text{boundaries}} = \big(V(\mathbf{r}) - V_{pp}(\mathbf{r})\big)\Big|_{\text{boundaries}}. \tag{2}$$

In practice, we employ the P^{3}D method to compute the Coulombic interaction in the first problem, which provides the electrostatic potential at any point in the simulation box while remaining both efficient and accurate. However, it is also possible to use the method developed by Genovese *et al.*[24] The Laplace equation of the second problem is solved in a similar approach used in the P^{3}D method. For a slab like geometry, Eq. (2) is applied only to boundary conditions in the nonperiodic direction, i.e., $z = 0$ and $z = L_z$. Section II B provides a brief summary of the P^{3}D method.

B. The P^{3}D method

Consider a set of N charged point particles with charges q_i, $i = \{1, \ldots, N\}$ at positions $\mathbf{r}_i$, with vanishing total charge, $\sum_{i=1}^{N} q_i = 0$, in a $L_x \times L_y \times L_z$ simulation box. Suppose that the particles are subjected to periodic boundary conditions in two dimensions (here: x and y) and to free boundary conditions in the third dimension (here: z). The total electric potential energy of these systems is given by

$$E = \frac{1}{2}{\sum_{\mathbf{n}}}' \sum_{i,j=1}^{N} \frac{q_i q_j}{|\mathbf{r}_{ij} + \mathbf{n}|}, \tag{3}$$

where $\mathbf{r}_{ij} = \mathbf{r}_i - \mathbf{r}_j$ and $\mathbf{n} = (n_x L_x, n_y L_y, 0)$ and n_x, n_y are integer values. Note for $\mathbf{n} = 0$ the term $i = j$ has to be excluded in the outer sum. Ewald[5] showed that Eq. (3) can be split into two parts, one of which decays rapidly in real space and the other involves a smooth charge density which can be treated very efficiently in Fourier space. Following Ewald's approach, we get

$$\begin{aligned} E = {} & \frac{1}{2}{\sum_{\mathbf{n}}}' \sum_{i,j=1}^{N} \left[\frac{q_i q_j}{|\mathbf{r}_{ij} + \mathbf{n}|} - \iint \frac{\rho_i(\mathbf{r}) \rho_j(\mathbf{r}' + \mathbf{n})}{|\mathbf{r} - \mathbf{r}'|} d\mathbf{r} d\mathbf{r}' \right] \\ & + \frac{1}{2} \sum_{\mathbf{n}} \sum_{i,j=1}^{N} \iint \frac{\rho_i(\mathbf{r}) \rho_j(\mathbf{r}' + \mathbf{n})}{|\mathbf{r} - \mathbf{r}'|} d\mathbf{r} d\mathbf{r}' \\ & - \frac{1}{2} \sum_{i=1}^{N} \iint \frac{\rho_i(\mathbf{r}) \rho_i(\mathbf{r}')}{|\mathbf{r} - \mathbf{r}'|} d\mathbf{r} d\mathbf{r}', \end{aligned} \tag{4}$$

where $\rho_i(r)$ are smooth spherical charge densities centered on the particles' positions. The standard choice in the Ewald method for the smooth atomic charge density is a Gaussian function,

$$\rho_i(\mathbf{r}) = \frac{q_i}{(\alpha^2 \pi)^{\frac{3}{2}}} \exp\left[-\frac{|\mathbf{r} - \mathbf{r}_i|^2}{\alpha^2} \right]. \tag{5}$$

Therefore, Eq. (4) can be rewritten as

$$E = E_{short} + E_{long} - E_{self},$$

where

$$E_{short} = \frac{1}{2}{\sum_{\mathbf{n}}}' \sum_{i,j=1}^{N} \frac{q_i q_j \operatorname{erfc}\left[\frac{|\mathbf{r}_{ij} + \mathbf{n}|}{\alpha \sqrt{2}} \right]}{|\mathbf{r}_{ij} + \mathbf{n}|}, \tag{6a}$$

$$E_{long} = \frac{1}{2} \sum_{\mathbf{n}} \sum_{i,j=1}^{N} \iint \frac{\rho_i(\mathbf{r}) \rho_j(\mathbf{r}' + \mathbf{n})}{|\mathbf{r} - \mathbf{r}'|} d\mathbf{r} d\mathbf{r}', \tag{6b}$$

$$E_{self} = \frac{1}{\alpha \sqrt{2\pi}} \sum_{i=1}^{N} q_i^2. \tag{6c}$$

The complementary error function in Eq. (6a) decays exponentially, and therefore, E_{short} can treated in a finite range by introducing a cutoff. Hence, the calculation of the first term can be done with linear scaling. The system is considered to have a nonzero charge density only within $[z_{lb}, z_{ub}]$ in the non-periodic direction, where $z_{ub} - z_{lb}$ is L_z plus twice the cutoff radius of the Gaussian charge density. The simulation cell in the periodic x and y directions on the other hand remains unaltered. Hence, consider the following effective simulation domain:

$$\mathcal{V} := [0, L_x] \otimes [0, L_y] \otimes [z_{lb}, z_{ub}]. \tag{7}$$

E_{long} is the electrostatic energy of the charge density comprised of a superposition of the atomic Gaussian functions. The corresponding electric potential, $V_{GF}(r)$, can be obtained by solving the following Poisson equation:

$$\nabla^2 V_{GF}(\mathbf{r}) = -4\pi \rho(\mathbf{r}), \tag{8}$$

where $\rho(\mathbf{r}) = \sum_{i=1}^{N} \rho_i(\mathbf{r})$. Eq. (8) is solved for the simulation cell given in Eq. (7) with periodic boundary conditions in x and y directions. We expand the potential function and the charge density in terms of a Fourier series,

$$V_{GF}(x, y, z) = \sum_{k,l=-\infty}^{\infty} c_{kl}(z) \exp\left[2i\pi \left(\frac{k\, x}{L_x} + \frac{l\, y}{L_y} \right) \right], \tag{9a}$$

$$\rho(x, y, z) = \sum_{k,l=-\infty}^{\infty} \frac{\eta_{kl}(z)}{-4\pi} \exp\left[2i\pi \left(\frac{k\, x}{L_x} + \frac{l\, y}{L_y} \right) \right]. \tag{9b}$$

Inserting Eqs. (9a) and (9b) in Eq. (8) yields

$$\left(\frac{d^2}{dz^2} - g_{kl}^2\right) c_{kl}(z) = \eta_{kl}(z), \tag{10}$$

where

$$g_{kl} := 2\pi\sqrt{\frac{k^2}{L_x^2} + \frac{l^2}{L_y^2}}. \tag{11}$$

In order to calculate the Fourier coefficients $c_{kl}(z)$ in Eq. (10), one needs to determine the boundary conditions at $z \to \pm\infty$. As explained in Ref. 8, we have $V(x, y, z \to \pm\infty) = \mp\beta$, where β is proportional to the dipole moment of the charge distribution along the z direction,

$$\beta = \frac{1}{2}\int_{z_{lb}}^{z_{ub}} \eta_{00}(z')z'dz'. \tag{12}$$

To deal with Eq. (10) employing above boundary conditions, one can write down the following conditions for the g's:

- $g_{00} = 0 \Rightarrow \frac{d^2}{dz^2}c_{00}(z) = \eta_{00}(z)$, we solve this differential equation with the boundary condition $c_{00}(z \to \pm\infty) = \mp\beta$.
- $g_{kl} \neq 0 \Rightarrow \left(\frac{d^2}{dz^2} - g_{kl}^2\right) c_{kl}(z) = \eta_{kl}(z)$, for all of these differential equations, we have to impose boundary conditions of the form $c_{kl}(z \to \pm\infty) = 0$.

$c_{00}(z)$ is constant for $z \notin [z_{lb}, z_{ub}]$, and therefore, one has to impose the Dirichlet boundary conditions $c_{00}(z_{lb}) = \beta$ and $c_{00}(z_{ub}) = -\beta$. As shown in Ref. 8, all differential equations with $|k| + |l| > 0$ must be solved subject to the Robin boundary conditions given by the following equations at z_{lb}:

$$c'(z_{lb}) - g_{kl}c(z_{lb}) = 0, \tag{13}$$

and at z_{ub}

$$c'(z_{ub}) + g_{kl}c(z_{ub}) = 0. \tag{14}$$

To solve the differential equations Eq. (10) with the boundary conditions explained above, the finite element method is employed as explained in Ref. 8 and its Appendix. Once the $c_{kl}(z)$ are obtained, the potential function is calculated using a reverse Fourier transform. Then, the electrostatic energy E_{long} and atomic forces can be calculated accordingly. The P^{3}D method provides values of the potential function at the upper and lower planes that are necessary to impose the boundary conditions of the second problem.

C. Laplace equation of the second problem

As illustrated in Sec. II A, the values of the potential function of the first problem at the boundaries need to be computed in order to solve the second problem. The potential function of the P^{3}D method is given by

$$V_{pp}(\mathbf{r}) = V_{GF}(\mathbf{r}) + \sum_{\mathbf{n}}\sum_{i=1}^{N} \frac{q_i \operatorname{erfc}\left[\frac{|\mathbf{r}_i - \mathbf{r} + \mathbf{n}|}{\alpha}\right]}{|\mathbf{r}_i - \mathbf{r} + \mathbf{n}|}. \tag{15}$$

The first term in Eq. (15) is directly available on all grid points based on our implementation of the P^{3}D method. If the grid points are chosen such that they lie exactly at the upper and lower boundaries, the first term can be obtained at no additional cost, without interpolation. The second term in Eq. (15) decays exponentially and it can be made finite ranged by introducing a cutoff. The Laplace equation must be solved subject to the following boundary conditions for the upper and lower planes, respectively:

$$V_{bup}(x, y) = V_{up} - V_{pp}(\mathbf{r})\big|_{z_{up}}, \tag{16}$$

$$V_{blp}(x, y) = V_{lp} - V_{pp}(\mathbf{r})\big|_{z_{lp}}. \tag{17}$$

In our implementation, the z coordinate of the lower and upper planes, z_{lp} and z_{up}, are 0 and L_z, respectively. In a similar approach as used in Sec. II B, we expand the potential function $V_s(\mathbf{r})$ in terms of a Fourier series in the x and y directions with expansion coefficients $f_{kl}(z)$. Replacing the Fourier series expansion in the Laplace equation yields

$$\left(\frac{d^2}{dz^2} - g_{kl}^2\right) f_{kl}(z) = 0, \tag{18}$$

where g_{kl} is given by Eq. (11). Eq. (18) differs from Eq. (10) in two aspects: first, it is homogeneous, and second, the boundary conditions are different. In order to obtain the boundary conditions of Eq. (18), $V_{bup}(x, y)$ and $V_{blp}(x, y)$ are expanded in terms of a Fourier series in the x and y directions with expansion coefficients a_{kl} and b_{kl}, respectively. Eq. (18) can be solved analytically and there is no need to employ the finite element method used for solving Eq. (10). $f_{00}(z)$ is a linear function given by

$$f_{00}(z) = \frac{(a_{00} - b_{00})\, z + (b_{00}\, z_{up} - a_{00}\, z_{lp})}{z_{up} - z_{lp}}, \tag{19}$$

and for $f_{kl}(z)$ with $|k| + |l| > 0$, we obtain

$$f_{kl}(z) = \frac{a_{kl}\, \sinh(g_{kl}(z - z_{lp})) + b_{kl} \sinh(g_{kl}(z_{up} - z))}{\sinh(g_{kl}(z_{up} - z_{lp}))}. \tag{20}$$

Using Eqs. (19) and (20), the $f_{kl}(z)$ are calculated on the grid points and subsequently $V_s(\mathbf{r})$ is obtained on the grid by performing a reverse Fourier transformation. The electrostatic energy contribution of the second problem is given by

$$E_s = \frac{1}{2}\sum_{i=1}^{N} q_i V_s(\mathbf{r}_i). \tag{21}$$

Since the exact potential $V_s(\mathbf{r})$ is unknown at the atomic coordinates, a Lagrange polynomial of order eight is used to interpolate the potential function. Finally, the total electrostatic energy is given by

$$E = E_{short} + E_{long} + E_{self} + E_s + \frac{L_x L_y (\Delta V)^2}{8\pi L_z},$$

where the first three terms are due to the electrostatic energy of point particles defined by Eqs. (6a)–(6c), and the fourth term is the electrostatic energy of the smooth potential given by Eq. (21). The last term is the electrostatic energy of the parallel plate capacitor whose plates are separated by a vacuum gap and the potential difference between them is ΔV.

III. NUMERICAL RESULTS

Here we present several numerical applications of the novel method to illustrate its accuracy and to demonstrate its potential to solve practical problems in atomistic simulations. The accuracy of the method is assessed by computing two relevant quantities when treating electrostatic point particles confined by metallic boundaries. First, we show the results of a convergence study with respect to the grid spacing. A fast and robust convergence in electrostatic energies is vital for an algorithm for solving the Poisson equation. Due to the use of Fourier series in the periodic directions, an exponential convergence rate is observed with respect to the grid spacing in the xy plane. However, a polynomial basis set is used in the non-periodic z-direction, and therefore, the convergence rate along z is algebraic $O(h_z^{2m})$, where m is the degree of the polynomial used in the finite element method. A detailed documentation of the finite element approach used in this study is given in Ref. 8. Fig. 2 illustrates the convergence rate in the total energy with respect to the grid spacing in the non-periodic direction, demonstrating that the relative error can be reduced down to machine precision.

Next, we studied the induced surface charge density on the metallic boundaries and how the choice of the grid affects this quantity. The total charge is calculated by numerically integrating the surface charge density according to[22]

$$Q_u = -Q_l = -\frac{1}{L_z}\sum_i q_i z_i + \frac{L_x L_y}{4\pi L_z}\Delta V,$$

where Q_u and Q_l are the total charges induced on the upper and lower metallic plates, respectively. Due to the translational invariance of the system in x and y directions, the total charge induced on the upper and lower planes must remain constant under all translations of the particles in the xy-plane. However, the total charge oscillates slightly due to the discretization of the equations. Fig. 3 shows these oscillation amplitudes with respect to the translation in the periodic directions for two different grid spacing in the periodic directions. The deviation from a constant value is very small. Furthermore,

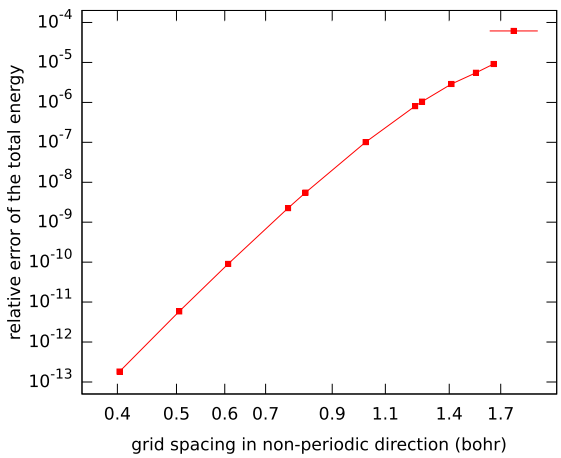

FIG. 2. Relative error in the total energy versus grid spacing in the z direction. On this double logarithmic plot, the curve has an asymptotic slope of 14 and an accuracy up to machine precision can be readily achieved.

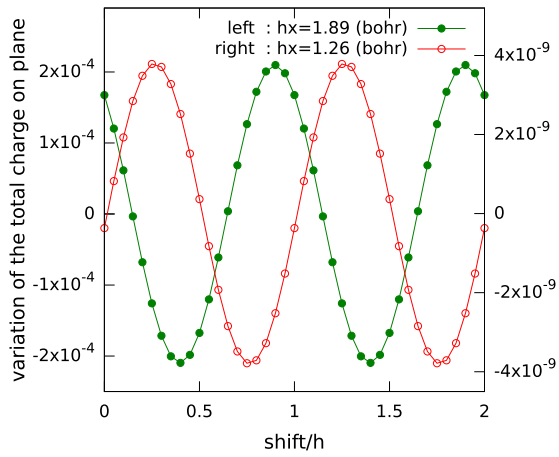

FIG. 3. Total induced charge on metallic plates versus shift of charged particles in a periodic direction for two different values of grid spacing.

the oscillation amplitude decays rapidly: it decreases by more than five orders of magnitude when the grid spacing is reduced by merely 30%.

Furthermore, we performed atomistic simulations of a NaCl system containing 1000 particles, where the short range interactions were modeled with the Born-Mayer-Huggins-Fumi-Tosi[25] (BMHFT) rigid-ion potential (see Ref. 26 for the complete parametrization). Several initial structures were prepared by randomly displacing the atoms from the pristine rock-salt structure with a small amplitude. Then, a local structural relaxation was performed for each of these configurations. Fig. 4 shows the total charge induced on the upper plane along the various minimization trajectories. All paths have the same total induced charge at the end of the relaxation since all pathways lead to the same, final rock-salt structure, even though the values differ significantly along the trajectories themselves. Obviously, the total induced charge in the final configurations would be different if the

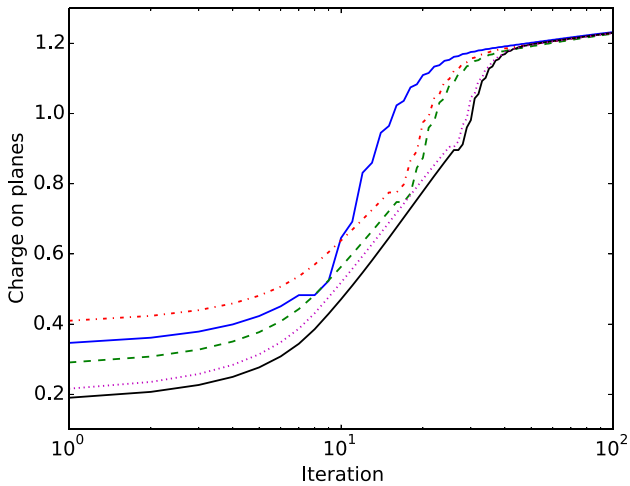

FIG. 4. Total charge induced on the metallic plates versus the iterations during a minimization process. Each curve represents different NaCl initial configuration in which particles were slightly randomly displaced from the rock-salt structure. The final value of the induced charge is independent of the trajectories since the final structure of all different initial configurations is the same.

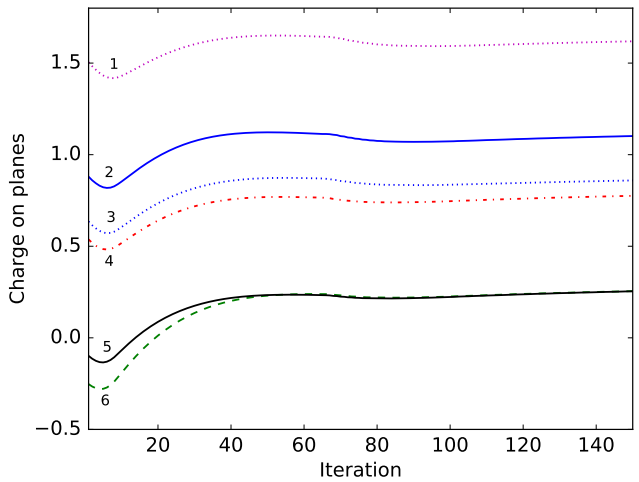

FIG. 5. Total charge induced on the metallic plates versus the iterations during a minimization process. Each curve represents different NaCl initial configuration with two Frenkel defects.

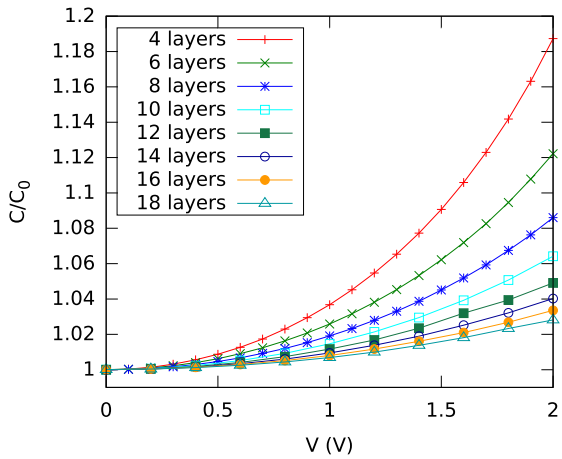

FIG. 6. Capacitance normalized to the capacitance at zero bias voltage versus potential difference of the two parallel metallic plates ($C_0 = \frac{dQ}{dV}|_{V=0}$).

structural relaxation lead to defect structures. To examine the effect of defects on charge accumulated at the metallic plates, we generated six 1000 atom rocksalt structures each with two Frenkel defects by randomly selecting atoms at different crystalline sites and moving them to random positions between atoms. We then relaxed the structures and plotted the charges on the plates along trajectories in Fig. 5. Defect configurations that relax to different final states lead to different charges on the plates. The pathways 5 and 6 converge to symmetrically equivalent structures.

We also investigated the response of a dielectric exposed to an external electric field. The typical approach in atomistic simulations to study an electric response is to apply an external uniform electric field. However, in experimental setups such electric fields are caused by a voltage difference of two electrodes surrounding the material. In ultrathin films, for example, the nonlinear response of the dielectric to the external electric field might have a large effect, which is completely neglected in the uniform electric field method. Furthermore, in practical situations, ions do not feel a homogeneous electric field, and thus, ionic displacements are indeed nonuniform. Also, ions in the vicinity of the interface between the dielectric and the electrodes feel an oscillatory electric field, and studying this phenomenon is not possible with the uniform electric field approach. Here we thus employ our novel method to study such a nonlinear dielectric behavior in thin NaCl films with between 4 and 18 atomic layers. Commonly, the nonlinear effects increase with increasing electric fields, and the response of the material to the electrostatic field (the total charge induced on upper/lower plane) is not a linear function of the bias voltage. Consequently, the capacitance is not a constant and it must be calculated through

$$C(V) = \frac{dQ(V)}{dV}.$$

Fig. 6 illustrates the ratio of the capacitance C and the capacitance at zero bias limit C_0 in terms of the bias voltage. Fig. 6 shows that the nonlinear contribution to capacitance increases strongly as a function of the bias voltage and it can be as high as 20% of the linear contribution. Based on the curves in Fig. 6, one would assume that the nonlinear contribution increases with the decrease of the film thickness. This is in fact not the case. In contrary: the nonlinear behavior is stronger for thicker films. Fig. 7 shows the ratio of C and C_0 in terms of the electric field. The electric field is calculated by the ratio of the potential difference between the two electrodes and their distance. From the curves in Fig. 7, one can see that the nonlinear contribution to the capacitance increases as the thickness of the film grows for a given value of electric field. However, the increase in the nonlinear contribution slows down for thick films and it is expected to approach zero at the limit of very thick films. Also, the electric fields used in Fig. 7 are much larger than the value for the electrical breakdown of bulk NaCl, and therefore, our results cannot be directly applied to the bulk material. However, the electrical breakdown of thin films is, in general, larger than that of bulk, justifying the use of such large electric fields in our calculations.

Finally, we calculated the dielectric constant of NaCl films as a function of their thickness. The dielectric properties of NaCl films are well known from *ab initio* studies,[27] employing the uniform external electric field technique. Combining our

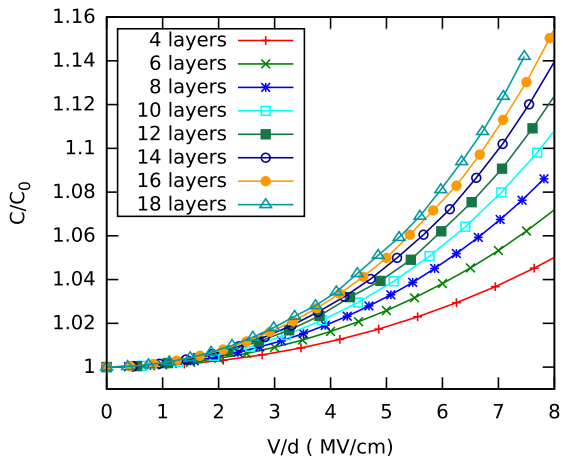

FIG. 7. Capacitance normalized to capacitance at zero bias voltage versus average external electric field due to the two parallel metallic plates.

TABLE I. Dielectric constant (K) of various NaCl ultrathin films as a function of the number of layers (n) in the film.

n	10	20	30	40	50	60	80	100
K	3.73	4.02	4.13	4.23	4.29	4.31	4.34	4.35

method and *ab initio* would thus be a compelling approach to further investigate dielectric properties of ionic ultrathin films confined with metallic plates. Table I presents the list of the dielectric constant for NaCl ultrathin films with a thickness of 10 to 100 layers using the BMHFT potential. The dielectric constants are obtained through the relation $K = \frac{C_0}{C_{vac}}$, where C_{vac} is the capacitance in the absence of the film. C_0 is the capacitance at the zero bias limit, where for thick films it is indeed virtually the same as the value obtained by the ratio of the total charge induced on the upper/lower planes to the potential difference of the two electrodes. An atomic relaxation with a very tight convergence criterion is required since the increasing number of particles in thick films leads to an ill-conditioned system which is hard to optimize. Table I indicates that the dielectric constant increases with the growth of the NaCl films; however, the rate slows down for thick films. It is expected that the dielectric constant approaches a fixed value which corresponds to the dielectric constant of bulk NaCl. Also, the quality of the interatomic potential has a strong influence on the accuracy of the dielectric constant. In the BMHFT potential, all ions are treated with fixed charges, and therefore, the dielectric constant obtained in our approach accounts only for the ionic degrees of freedom and does not include the effects due to the electronic polarization.

IV. SCALING

As mentioned in Sec. II, our algorithm inherits the scaling behavior of the P^{3}D method, i.e., $O(N \ln(N))$. The additional cost due to considering metallic boundary conditions is at most half of the total computational time for the P^{3}D method. We compared the computational cost of the ICMMM2D method, as implemented in the ESPResSo[28] package, with our new method. Both methods result in the identical values for the atomic forces and total energies when the appropriate parameters are tuned. We chose parameters that lead to a maximal relative error in atomic forces of less than 10^{-4}, and also lead to a fair comparison with respect to the computational cost. Fig. 8 shows the CPU time for calculating the electrostatic interactions using the following methods: MMM2D, ICMMM2D, P^{3}D, and P^{3}D with parallel plates. The systems, which were used for the benchmarking of the computational cost, consist of 28, 64, 512, 4096, and 32 768 atoms, with a nearly uniform increase of the system in all three dimensions. In the calculations with ESPResSo, the number of layers in the MMM2D and ICMM2D methods were optimized for the cell size in the nonperiodic direction in order to obtain minimal computational cost. As an example, for the system with 64 atoms and a slab thickness of 17 Å in the nonperiodic direction, 10 layers were used. The results

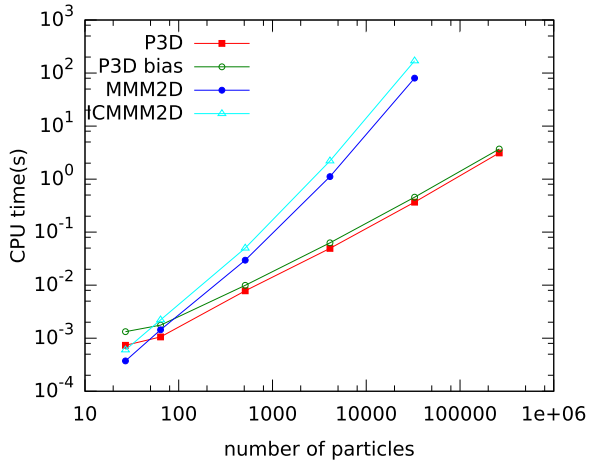

FIG. 8. CPU time of single force evaluation as a function of the number of particles in the simulation box.

show a complexity which is close to the theoretical scaling, i.e., $O(N^{5/3})$. In the P^{3}D method, the Gaussian width was set to 2.063 Å while the mesh sizes in the periodic and nonperiodic directions were 1.375 and 1.22 Å, respectively. As it can be deduced from Fig. 8, the method presented in this paper is more efficient than the ICMMM2D method, and it is indeed faster than the ICMMM2D method for systems containing more than 50 particles. It is worth mentioning that the increase in computational cost due to the presence of parallel metallic plates is less in the P^{3}D method which employs the superposition principle as compared to the ICMMM2D method which uses the method of image particles.

V. CONCLUSION

In summary, we have developed a new method for evaluating the electrostatic interaction of charged point particles confined between two parallel metallic plates. Due to the linear nature of the governing electrostatic equations, the electric potential is assumed to be a superposition of two parts; the first part in the absence of the metallic plates due to the point charges in the simulation cell, and the second with a smooth potential, imposed by the metallic boundaries. Using this approach, our method can be combined with any available methods for treating 2D geometries in systems without metallic plates. Our results show that the proposed method is very efficient and exhibits a quasilinear scaling, $O(N \ln(N))$. In order to investigate the accuracy and efficiency of the method, we performed atomistic simulations of NaCl systems. The relative error of the total energy, which depends on the grid spacing, decreases very rapidly with increasing mesh size and can be readily reduced to machine precision. Furthermore, by imposing the potential difference between metallic plates and allowing the system to relax, the nonlinear behavior of the capacitance in ultrathin films of NaCl was investigated. The nonlinear contribution grows as the number of layers in the film increases; however, it decreases as the film thickness increases. In addition, we calculated the dielectric constant of NaCl ultrathin films,

showing that the dielectric constant increases with the film thickness: the dielectric constant of films with 100 layers is about 20% lower than experimental dielectric constant of bulk NaCl.

[1]V. Aravindan, J. Gnanaraj, Y.-S. Lee, and S. Madhavi, Chem. Rev. **114**, 11619 (2014).
[2]S. Naserifar, L. Liu, W. A. Goddard III, T. T. Tsotsis, and M. Sahimi, J. Phys. Chem. C **117**, 3308 (2013).
[3]L. Greengard and V. Rokhlin, J. Comput. Phys. **73**, 325 (1987).
[4]A. Neelov, S. A. Ghasemi, and S. Goedecker, J. Chem. Phys. **127**, 024109 (2007).
[5]P. P. Ewald, Ann. Phys. **64**, 253 (1921).
[6]R. Sperb, Mol. Simul. **20**, 179 (1998).
[7]A. Arnold and C. Holm, Comput. Phys. Commun. **148**, 327 (2002).
[8]S. A. Ghasemi, A. Neelov, and S. Goedecker, J. Chem. Phys. **127**, 224102 (2007).
[9]A. Arnold, J. de Joannis, and C. Holm, J. Chem. Phys. **117**, 2496 (2002).
[10]J. de Joannis, A. Arnold, and C. Holm, J. Chem. Phys. **117**, 2503 (2002).
[11]D. M. Heyes, M. Barber, and J. H. R. Clarke, J. Chem. Soc., Faraday Trans. 2 **73**, 1485 (1977).
[12]J. Hautman and M. L. Klein, Mol. Phys. **75**, 379 (1992).
[13]B. R. A. Nijboer, Physica A **125**, 275 (1984).
[14]E. Spohr, J. Chem. Phys. **107**, 6342 (1997).
[15]Y. J. Rhee, J. W. Halley, J. Hautman, and A. Rahman, Phys. Rev. B **40**, 36 (1989).
[16]I. C. Yeh and M. L. Berkowitz, J. Chem. Phys. **111**, 3155 (1999).
[17]S. Tyagi, A. Arnold, and C. Holm, J. Chem. Phys. **127**, 154723 (2007).
[18]S. Tyagi, M. Süzen, M. Sega, M. Barbosa, S. Kantorovich, and C. Holm, J. Chem. Phys. **132**, 154112 (2010).
[19]S. Tyagi, A. Arnold, and C. Holm, J. Chem. Phys. **129**, 204102 (2008).
[20]D. Boda, D. Gillespie, W. Nonner, D. Henderson, and B. Eisenberg, Phys. Rev. E **69**, 046702 (2004).
[21]J. Hautman, J. W. Halley, and Y.-J. Rhee, J. Chem. Phys. **91**, 467 (1989).
[22]K. Takae and A. Onuki, J. Chem. Phys. **139**, 124108 (2013).
[23]J. W. Perram and M. A. Ratner, J. Chem. Phys. **104**, 5174 (1996).
[24]L. Genovese, T. Deutsch, and S. Goedecker, J. Chem. Phys. **127**, 054704 (2007).
[25]M. P. Tosi and F. G. Fumi, J. Phys. Chem. Solids **25**, 45 (1964).
[26]F. H. Ree and A. C. Holt, Phys. Rev. B **8**, 826 (1973).
[27]T. Ono and K. Hirose, Phys. Rev. B **72**, 085105 (2005).
[28]H. Limbach, A. Arnold, B. Mann, and C. Holm, Comput. Phys. Commun. **174**, 704 (2006).